INSTITUTE OF PHYSICS PUBLISHING JOURNAL OF PHYSICS B: ATOMIC, MOLECULAR AND OPTICAL PHYSICS

J. Phys. B: At. Mol. Opt. Phys. **38** (2005) 189–205 doi:10.1088/0953-4075/38/3/005

Total and ionization cross sections of electron scattering by fluorocarbons

B K Antony[1], K N Joshipura[1] and N J Mason[2]

[1] Department of Physics, Sardar Patel University, Vallabh Vidyanagar-388 120, Gujarat, India
[2] Department of Physics & Astronomy, Open University, Milton Keynes-MK7 6AA, UK

E-mail: bk_antony@rediffmail.com

Received 7 August 2004
Published 24 January 2005
Online at stacks.iop.org/JPhysB/38/189

Abstract

Electron impact total cross sections (50–2000 eV) and total ionization cross sections (threshold to 2000 eV) are calculated for typical plasma etching molecules CF_4, C_2F_4, C_2F_6, C_3F_8 and CF_3I and the CF_x ($x = 1$–3) radicals. The total elastic and inelastic cross sections are determined in the spherical complex potential formalism. The sum of the two gives the total cross section and the total inelastic cross section is used to calculate the total ionization cross sections. The present total and ionization cross sections are found to be consistent with other theories and experimental measurements, where they exist. Our total cross section results for CF_x ($x = 1$–3) radicals presented here are first estimates on these species.

(Some figures in this article are in colour only in the electronic version)

1. Introduction

The semiconductor plasma industry remains a multi-billion worldwide industry that underpins much of modern technology and engineering. It is an industry and technology that is capable of considerable growth in the next decade with the development of a new generation of micro and nanosystem technologies (MST) [1–4]. MST devices are silicon based and incorporate features that cover a range of scales from fractions of a millimetre down to a few nanometres, the latter are the first examples of exploitation of nanotechnology by modern industry. Tailoring processes for the plasma etching of silicon is therefore of particular importance for a wide variety of MST demands. Key developments include robust and reliable control of atomic-order surface adsorption, surface diffusion and surface reactions in plasma etch processes [5]. These surface mechanisms control the vertical and lateral etch rates as well as the etch selectivity, all of which must be optimized in order to fabricate functional structures. Currently, there are two approaches to controlling plasma–surface interactions in such an

etching environment: one seeks to use chemistry; the other is based on control engineering and both now seek to achieve nanoscale resolution [6].

Control of the plasma processing methodology can only occur through the thorough understanding of the properties of plasmas. However, many plasma processes are currently used by industry without a complete understanding of the chemical and physical properties of the plasma involved, thus they are non-predictive and hence it is not possible to alter the manufacturing process without the risk of considerable product loss. Indeed, plasma process control remains largely rudimentary and is performed predominantly by trial and error, an expensive procedure which limits growth and innovation of the industry [7]. A clear research imperative in the next decade will therefore be to increase our knowledge of the chemical and other interactions in such plasmas of electrons, ions and radicals with neutral species [7]. A more comprehensive understanding of such processes will then allow models [8] of such plasmas to be constructed that may be used to design the next generation of plasma reactors, reactors that

(i) will allow more site specific control on surface reactivity and
(ii) may be more efficient in the use of materials.

The latter is particularly important since most of the current feed gases are known *greenhouse gases* and the leakage of effluent from such plasmas is now recognized to be a major contributor to the appearance of such greenhouse gases in the terrestrial atmosphere. This in turn has led to international agreement (under the Kyoto protocol) to phase out the use of such feed gases and seek their replacement with cleaner alternatives by 2008 [4, 9]. Hence, there is now a worldwide research programme to study the physical and chemical processes that underpin those plasmas that etch the surfaces of silicon.

The total cross sections (TCS) calculated in this paper are in the energy range from 50 to 2000 eV. Hence, present TCS are not directly applied to technological plasma. Nevertheless, the most fundamental processes in any plasma and the rate determining step in any etchant process are the *dissociative and ionization* processes that produce the charged species to sustain the plasma. Such processes are driven by electron interactions [10]. In this context, present calculations of total ionization cross sections find importance. Our knowledge of electron interactions with many of gases used in the semiconductor industry remains fragmentary. Recently, Christophorou and co-workers [11] have published several reviews of the datasets for the most commonly used semiconductor gases but note that data on many of the secondary species produced in the plasma (e.g., radicals) are lacking. Furthermore, as the industry seeks to explore the use of alternative feedstock gases (with reduced environmental consequences), the need for an expanded database encompassing several dozen compounds becomes more pressing. Collection of experimental data is time consuming and there are currently only a few research groups worldwide that can conduct such experiments [12]. Therefore, there has been an increasing emphasis on the development of theoretical methods to provide such data. However, a complete electron scattering calculation (as demonstrated by the R matrix method [13, 14]) is also time consuming and restricted to small molecular systems. Accordingly, simpler approximate theories have been developed capable of delivering cross sections (rate constants) quickly albeit with restricted accuracy. Such data are proving to be useful to the semiconductor industry as they develop models of the plasma process to judge which alternative feedstock gases might be used in 'field' trials.

Towards this goal, we report a new simple method aimed at providing an estimate of both the total elastic and inelastic cross sections for electron scattering from molecules from which ionization cross sections may be derived. The results of such calculations are compared both with experiment (where available) and other calculations. We do not claim that the

results derived by such methodology are 'definitive' but will provide a useful guideline to the magnitude and shape of the cross section at intermediate and high incident energies for any target, including radicals and other chemically unstable but highly reactive species wherein the experimental uncertainties could also be high.

2. Theoretical

Total elastic (Q_{el}) and inelastic (Q_{inel}) cross sections are generated using a spherical complex potential formalism [15–19]. The total cross section (Q_{T}) is then obtained by summing the individual elastic and inelastic cross sections, i.e.

$$Q_{\mathrm{T}}(E_{\mathrm{i}}) = Q_{\mathrm{el}}(E_{\mathrm{i}}) + Q_{\mathrm{inel}}(E_{\mathrm{i}}). \tag{1}$$

The total cross section Q_{T} we discuss here is rotationally and vibrationally elastic. Rotational and vibrational excitation are predominantly 'resonant' driven processes, and therefore add only a small contribution to the total cross sections, in the present energy range of 50–2000 eV. Our focus is on ionization in relation to other processes induced by electrons. We are restricted to a lower limit of 50 eV for the total cross section because our total elastic cross section is reliable above this energy only. This is due to the exchange and polarization potentials [16] we use, which are not strictly valid near and below this energy. In contrast the total inelastic cross sections can be calculated at these energies because the polarization effect has negligible contribution to the real part (equation (4) to follow) of the complex potential. Molecular electric dipole polarizabilities employed here were obtained for stable molecules using the Hartree–Fock method and the analytical method for polarizabilities [20] in the program GAMESS [21]. Bond distances and angles were taken to be the experimental values. The basis sets used[3] were Sadlej's pVTZ C, F (10s, 6p, 4d) → [5s, 3p, 2d] [22], I (19s, 15p, 12d, 4f) → [11s, 9p, 6d, 2f] [23]) as these basis sets were especially designed to reproduce molecular electrical properties, particularly polarizabilities. For CF_x radicals, the programs DALTON [24] and MOLCAS [25] were used.

To obtain the total ionization cross section Q_{ion} a semi-empirical approach [16–19] called the 'complex scattering potential–ionization contribution' (CSP-*ic*) method is applied to derive it from the calculated Q_{inel}. The total inelastic cross section Q_{inel} may be partitioned as

$$Q_{\mathrm{inel}}(E_{\mathrm{i}}) = Q_{\mathrm{ion}}(E_{\mathrm{i}}) + \sum Q_{\mathrm{exc}}(E_{\mathrm{i}}) \tag{2}$$

with Q_{ion} the total cross section for all allowed ionization processes and $\sum Q_{\mathrm{exc}}$ the sum over total excitation cross sections for all accessible electronic transitions. The second term arises mainly from the low-lying dipole allowed transitions for which the cross section decreases rapidly at higher energies. The quantity $\sum Q_{\mathrm{exc}}$ becomes less important than Q_{ion} at energies well above the ionization threshold [26]. Hence, we can write

$$Q_{\mathrm{inel}}(E_{\mathrm{i}}) \geqslant Q_{\mathrm{ion}}(E_{\mathrm{i}}). \tag{3}$$

Our theoretical procedure starts with the formulation of the complex potential of the target system. This scattering potential is derived from the spherically averaged charge densities of the target molecules, as explained in our earlier work [18, 19].

Presently, we make use of the 'group additivity method' [27] to find the total cross section of the molecule after finding the cross section for each group in the molecule (e.g., the

[3] Basis sets were obtained from the Extensible Computational Chemistry Environment Basis Set Database, Version 6/19/03, as developed and distributed by the Molecular Science Computing Facility, Environmental and Molecular Sciences Laboratory which is part of the Pacific Northwest Laboratory, PO Box 999, Richland, WA 99352, USA, and funded by the US Department of Energy. The Pacific Northwest Laboratory is a multi-program laboratory operated by Battelle Memorial Institute for the US Department of Energy under contract DE-AC06-76RLO 1830.

two $-CF_2$ groups in C_2F_4). That is, cross section contributions arising from these centres are then added together to obtain the total cross section. Such an approximation is justified by the fact that the C–C bond length is much larger than the C–F bond length, where the modified additive method is reasonable. This method is better than the simple atomic additivity rule in view of the larger bond length and the present energy range.

In the present method the interference effect between these chemical groups is not considered. This effect may be important below 100 eV or so as the de Broglie wavelength of electron ($\sim$1.23 Å) will be comparable to the bond length (e.g., the C–C bond length of C_2F_6 is 1.54 Å). This might lead to an overestimation of the calculated cross sections. However, we will see in section 3 that such an effect is negligible in the present calculations. Moreover, in the case of C_2F_4 (figure 3) the present Q_T is below the measurements and other theories. Thus, we have not made any effort to modify the present method to include effects like interference. Besides this, the present method is more valid due to the presence of the F atom, which is known to be a weak scatterer. Further, in the ionization the molecular ion formed in the exit channel usually has larger bond lengths compared to the neutral target molecule. Also, the single-centre target charge density for each group is obtained by a linear combination of constituent atomic charge densities, renormalized to account for covalent bonding and the total number of electrons present in that molecular group [19]. This makes our approximation reasonable.

We had assumed two or three centres or groups, depending on the structure of the molecule [28, 29]. These centres were at the C atoms for all molecules, except for CF_3I where we have one more centre about the heavier I atom. Using the obtained molecular charge density we construct the real part of the complex potential [16, 17] $V_{opt} = V_R + iV_I$, which is the sum of static (V_{st}), exchange (V_{ex}) and polarization (V_p) potentials,

$$V_R = V_{st}(r) + V_{ex}(r, E_i) + V_p(r, E_i). \tag{4}$$

The imaginary part (V_I) accounts for the total loss of scattered flux into all the allowed channels of electronic excitation and ionization. We have used a model potential, given by Staszewska *et al* [30], which is a quasi-free, Pauli-blocking, dynamic absorption potential (V_{abs}) given in au as

$$V_{abs}(r, E_i) = -\tfrac{1}{2}\rho(r)v_{loc}\sigma_{ee}$$

which can be rewritten as

$$V_{abs}(r, E_i) = -\rho(r)\left(\frac{T_{loc}}{2}\right)^{1/2}\left(\frac{8\pi}{10k_F^3 E_i}\right)\theta\big(p^2 - k_F^2 - 2\Delta\big)(A_1 + A_2 + A_3). \tag{5}$$

Here v_{loc} is the local speed of the incident electron and σ_{ee} denotes the average total cross section of the binary collision of the incident electron with a target electron. The local kinetic energy of the incident electron is obtained from

$$T_{loc} = E_i - V_R = E_i - (V_{st} + V_{ex} + V_p). \tag{6}$$

In equation (4), $p^2 = 2E_i$, k_F is the Fermi wave vector and Δ is an energy parameter. $\theta(x)$ is the Heaviside step function, such that $\theta(x) = 1$ for $x > 0$, and is zero otherwise. The dynamic functions A_1, A_2 and A_3 which are given in Staszeweska *et al* [30] depend differently on $\rho(r)$, I, Δ and E_i. The parameter Δ assumed to be fixed in the original model determines a threshold below which $V_{abs} = 0$, and the ionization or excitation is prevented energetically. Here, we have modified Δ such that at impact energies close to the (vertical) ionization threshold I, excitations to the discrete states also take place, but as E_i increases valence ionization becomes dominant, together with the possibility of ionization from the inner electronic shells. In the range of intermediate energies the V_{abs} shows a rather excessive loss

of flux into the inelastic channels. The potential also penetrates the region of inner electronic shells, which are of course harder to excite or ionize. In order to rectify this behaviour of this potential, we choose $\Delta \approx I$ for low E_i and $\Delta > I$ at E_i near the position of the peak of Q_{inel}. Thus, our modification [16, 17] expresses Δ as a slowly varying function of E_i around I.

The Schrödinger equation is then solved with this complex optical potential, using the appropriate boundary conditions by partial wave analysis. The real and imaginary parts of the phase shifts $\delta_l = \mathrm{Re}\,\delta_l + \mathrm{i}\,\mathrm{Im}\,\delta_l$ are generated for various partial waves l. Thus, we get the S-matrix elements,

$$S_l = \exp(2\mathrm{i}\delta_l) \tag{7}$$

which can be written presently as

$$S_l = \eta_l \exp(2\mathrm{i}\,\mathrm{Re}\,\delta_l) \tag{8}$$

where the quantity $\eta_l = \exp(-2\,\mathrm{Im}\,\delta_l)$ is called the 'inelasticity' or 'absorption' factor [31]. The term absorption being understood in the sense that particle disappears from incident channel. Using this complex phase shifts the total elastic cross section is calculated as given by Joachain [31]

$$Q_{el} = \frac{\pi}{k^2} \sum_{l=0}^{\infty} (2l+1)|\eta_l \exp(2\mathrm{i}\,\mathrm{Re}\,\delta_l) - 1|^2 \tag{9}$$

and the total inelastic cross section,

$$Q_{inel} = \frac{\pi}{k^2} \sum_{l=0}^{\infty} (2l+1)\left(1 - \eta_l^2\right). \tag{10}$$

The total cross section Q_T follows from equation (1). The inelastic cross section Q_{inel} thus calculated within the quantum mechanical approximation of partial wave formalism is the high energy limit of Q_{ion}, which is required in plasma applications. Presently, we extract Q_{ion} from Q_{inel}. There is no rigorous way to get the former from the latter. A theoretical basis of the present semi-empirical formalism is provided by the dominance of the continuum scattering channel over the discrete ones, at $E_i > I$. In order to determine Q_{ion} from our calculated Q_{inel}, we define the following quantity for $E_i \geqslant I$.

$$R(E_i) = \frac{Q_{ion}(E_i)}{Q_{inel}(E_i)} \tag{11}$$

such that $0 \leqslant R \lesssim 1$. We require that $R = 0$ when $E_i \leqslant I$. For a number of stable molecules such as O_2, H_2O, CH_4, SiH_4, etc, for which the experimental cross sections Q_{ion} are known accurately [16, 17], the ratio R rises steadily as the energy increases above the threshold, and it is found that

$$R(E_i) \begin{cases} = R_p, & \text{at} \quad E_i = E_p \\ \cong 1, & \text{for} \quad E_i \gg E_p \end{cases} \tag{12}$$

where E_p stands for the incident energy at which the calculated Q_{inel} attains its maximum. R_p stands for the value of R at $E_i = E_p$. The above behaviour is attributed to the faster fall of the second term $\sum Q_{exc}$ in equation (2) and as per our discussion [16–18] we choose $R_p \cong 0.7$. This choice follows from the general observation that at energies close to the peak of the ionization cross section the contribution of the molecular Q_{ion} is about 70–80% of the total inelastic cross sections Q_{inel}. The value of R_p as 0.7 or 0.8 introduces an uncertainty of about 7% at the average value of $R_p = 0.75$, as against the usual experimental errors of about 10–15% observed in many cases. The higher limit of the ratio, i.e., 80%, is observed only in the targets having very high ionization potentials such as Ne ($I = 21.56$ eV) [15]. The molecules discussed

Table 1. Target properties [28, 29] and parameters used in equation (13).

			Parameters		
Target	I (eV)	E_p (eV)	a	C_1	C_2
CF_4	16.90	125	14.5279	−1.5031	−10.3303
C_2F_4	10.12	115	19.9137	−1.7237	−12.1332
C_2F_6	13.60	135	17.7751	−1.6338	−11.4918
C_3F_8	13.70	130	15.9641	−1.5455	−10.9765
CF_3I	10.23	90	16.1054	−1.5653	−10.9282
CF	9.11	100	6.6075	−0.6484	−11.7323
CF_2	11.44	125	6.4605	−0.6615	−11.2774
CF_3	8.90	120	7.7177	−0.5741	−15.1857

in this paper have ionization potentials ranging from 8.90 to 13.70 eV (except CF_4 with $I = 16.19$ eV), hence, we have selected the lower limit of 70%. We emphasize that the value of R_p compared to a particular experiment or theory may vary from target to target and from one investigation to another, but the present choice preserves the generality of our method [19].

For calculating the Q_{ion} from Q_{inel} we need R as a continuous function of energy $E_i \geqslant I$, hence we represent [16, 17] the ratio R in the following manner:

$$\begin{aligned} R(E_i) &= 1 - f(U) \\ R(E_i) &= 1 - C_1 \left[\frac{C_2}{U + a} + \frac{\ln(U)}{U} \right]. \end{aligned} \tag{13}$$

Here, U is the dimensionless variable defined through $U = \frac{E_i}{I}$.

The functional form of $f(U)$ in equation (13) is adopted from the fact that, as E_i increases above I, the ratio R increases and approaches unity, since the ionization contribution rises and the discrete excitation term in equation (1) decreases. The discrete excitation cross sections, dominated by dipole transitions, fall off as $U^{-1}\ln(U)$ at high energies. Accordingly, the decrease of the function $f(U)$ must also be proportional to $U^{-1}\ln(U)$ in the high range of energy. However, the two-term representation of $f(U)$ given in equation (11) is more appropriate since the first term in the square bracket ensures a better energy dependence at low and intermediate E_i. Equation (13) involves dimensionless parameters C_1, C_2 and 'a' that reflect the target properties indirectly through the use of ionization potential in U and geometry in charge density. To determine these parameters, we note the following three conditions on the ratio R. (i) It is zero at and below the ionization threshold, (ii) it behaves in accordance with equation (12) at the peak position E_p and (iii) it approaches 1 asymptotically for E_i sufficiently larger than E_p. These parameters are exhibited in table 1 for the present molecules. Equations (11)–(13) define the present CSP-*ic* approach [16–18].

3. Results and discussion

3.1. Stable molecules

The theoretical approach discussed above may be used to estimate values of Q_T and Q_{ion} for any molecular target including radicals. We have tested our approximations by calculating Q_T and Q_{ion} for molecules for which there exist reasonably well-established experimental datasets (e.g., CF_4 [17]). The presently derived values of Q_T are compared with the additivity (AR) and modified additivity (EGAR—energy-dependent geometric additivity rule) results of Jiang *et al* [32]. Q_{ion} is compared with two other approximate formalisms,

Table 2. Q_{ion} and Q_T (in Å^2) for C_2F_4, C_2F_6, C_3F_8 and CF_3I.

	C_2F_4		C_2F_6		C_3F_8		CF_3I	
E_i (eV)	Q_{ion}	Q_T	Q_{ion}	Q_T	Q_{ion}	Q_T	Q_{ion}	Q_T
20	1.29	–	0.93	–	1.09	–	3.11	–
30	2.75	–	2.66	–	3.79	–	6.01	–
40	3.89	–	4.20	–	6.20	–	7.53	–
50	4.71	23.61	5.57	33.29	8.26	42.28	8.39	32.46
60	5.33	23.43	6.64	32.32	9.80	41.22	8.88	29.60
70	5.71	23.10	7.44	30.97	10.90	39.62	9.10	27.08
80	5.97	22.58	8.00	29.57	11.65	37.62	9.20	25.02
90	6.09	21.89	8.43	28.17	12.17	35.91	9.23	23.27
100	6.16	21.14	8.69	26.90	12.47	34.63	9.18	22.06
150	6.09	17.60	8.95	22.15	12.54	29.40	8.58	18.52
200	5.82	15.53	8.58	19.51	11.94	25.78	7.91	16.49
300	5.21	12.97	7.53	16.07	10.51	21.18	6.90	13.90
400	4.68	11.17	6.69	13.94	9.36	18.29	6.15	12.21
500	4.26	9.81	5.97	12.24	8.50	16.28	5.57	11.00
600	3.94	8.83	5.42	10.93	7.77	14.58	5.09	9.80
700	3.69	7.98	4.96	9.87	7.15	13.15	4.70	8.86
800	3.44	7.36	4.58	9.00	6.61	12.08	4.38	8.15
900	3.26	6.78	4.21	8.28	6.14	11.16	4.11	7.43
1000	3.11	6.28	3.93	7.67	5.74	10.38	3.88	6.86
1500	2.47	4.34	2.92	5.48	4.29	7.67	3.00	4.86
2000	2.04	3.66	2.28	4.40	3.38	6.16	2.67	3.60

binary-encounter–Bethe or BEB method [33, 34] and the Deutsch–Märk (DM) method [35]. Both Q_T and Q_{ion} are also compared with the values recommended by Christophorou [11] wherever available. The cross sections for the molecules C_2F_4, C_2F_6, C_3F_8 and CF_3I are shown in table 2. The values for CF_4 are included in table 3 along with its constituent CF_x ($x = 1$–3) radicals.

Our calculated total cross sections Q_T for the well-known tetrahedral target CF_4 are presented in figure 1. Good agreement is found with the theoretical values of Jiang *et al* [36] and the recommended values of Christophorou *et al* [37] above 150 eV. The measurements of Zecca *et al* [38] and Nishimura *et al* [39] agree with our calculated values at energies above 150 eV but the values of Sueoka *et al* [40] are lower at all energies. Methods like EGAR, which seem to agree with experimental data, do not add to our understanding of collision processes at low energies. Hence, we have not attempted to modify the AR at low E_i.

In figure 2, our present ionization results for CF_4 are compared with BEB theory [33], the recommended ionization cross sections from Christophorou and Olthoff [41], and measurements of Poll *et al* [42] and Nishimura *et al* [43]. The present results are very close to BEB theory [33] and the recommended cross section [41] at all energies, except that at the peak the BEB values are slightly lower. The experiments of Poll *et al* are higher than all the other results presented here, but all the theories are within the experimental error limit (15%) of this measurement. The experimental values of Nishimura *et al* are slightly lower than the theories at energies ranging from 50 to 400 eV, but in good agreement with our results at all other energies.

In figure 3, we have plotted the total cross section Q_T of C_2F_4 along with the theoretical values of Jiang *et al* [32]. The AR is the simple additive rule which is obviously higher than that of the EGAR which is the energy-dependent geometric additivity rule. Both methods overestimate the cross section at intermediate energies, while they merge with the present

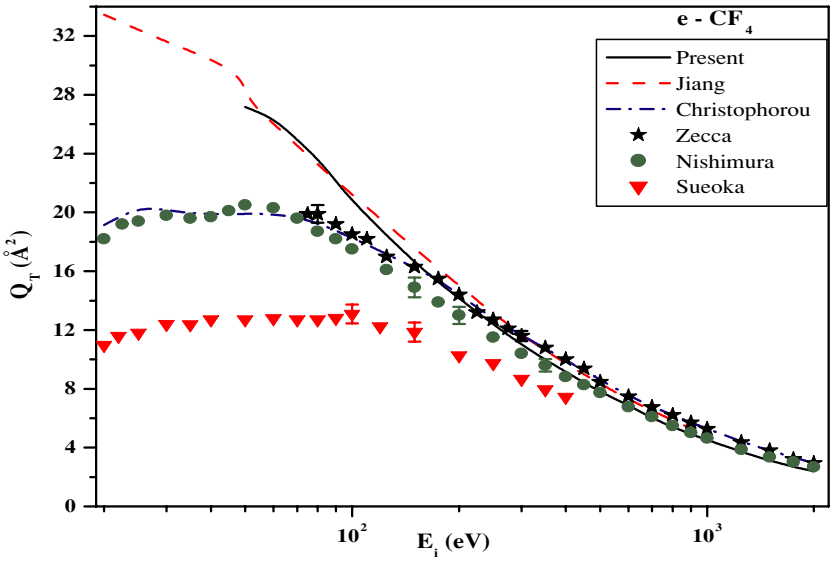

Figure 1. Total cross sections for e–CF_4 scattering. The solid line represents the present results. Dash—Jiang *et al* [36] (theory); dashed–dotted—Christophorou *et al* [37] (recommended); ⋆—Zecca *et al* [38] (experiment); filled circles—Nishimura *et al* [39] (experiment); filled inverted triangles—Sueoka *et al* [40] (experiment).

Table 3. Q_{ion} and Q_T (in Å^2) for CF_x radicals and their parent molecule CF_4.

	CF		CF_2		CF_3		CF_4	
E_i (eV)	Q_{ion}	Q_T	Q_{ion}	Q_T	Q_{ion}	Q_T	Q_{ion}	Q_T
20	1.019	–	0.707	–	0.975	–	0.19	–
30	1.787	–	1.546	–	1.979	–	1.37	–
40	2.322	–	2.248	–	2.854	–	2.58	–
50	2.689	13.166	2.747	19.948	3.582	25.682	3.43	27.18
60	2.973	12.096	3.206	17.919	4.125	23.459	4.16	26.43
70	3.143	11.236	3.513	16.422	4.555	21.414	4.73	24.95
80	3.232	10.476	3.728	15.161	4.891	19.670	5.10	23.65
90	3.277	9.646	3.867	14.081	5.098	18.323	5.37	22.15
100	3.294	8.979	3.954	13.254	5.279	17.243	5.54	20.76
150	3.185	7.112	3.981	10.807	5.479	14.168	5.71	16.54
200	2.943	6.102	3.745	9.172	5.359	12.209	5.41	14.12
300	2.529	4.780	3.217	7.039	4.800	9.484	4.63	10.94
400	2.206	3.959	2.829	5.737	4.259	7.784	4.09	9.16
500	1.960	3.388	2.556	4.862	3.805	6.609	3.60	7.77
600	1.757	2.967	2.312	4.227	3.431	5.746	3.20	6.88
700	1.591	2.640	2.141	3.738	3.115	5.079	2.93	6.01
800	1.456	2.380	1.972	3.352	2.854	4.554	2.68	5.40
900	1.341	2.168	1.831	3.039	2.626	4.125	2.48	4.91
1000	1.244	1.992	1.713	2.781	2.435	3.772	2.27	4.51
1500	0.914	1.491	1.259	1.892	1.745	2.597	1.67	3.06
2000	0.731	1.096	1.011	1.498	1.386	2.019	1.25	2.39

values at high energies. The experimental results of Szmytkowski *et al* [44] are also plotted and are higher than the present results over most of the energy range, but are surprisingly lower

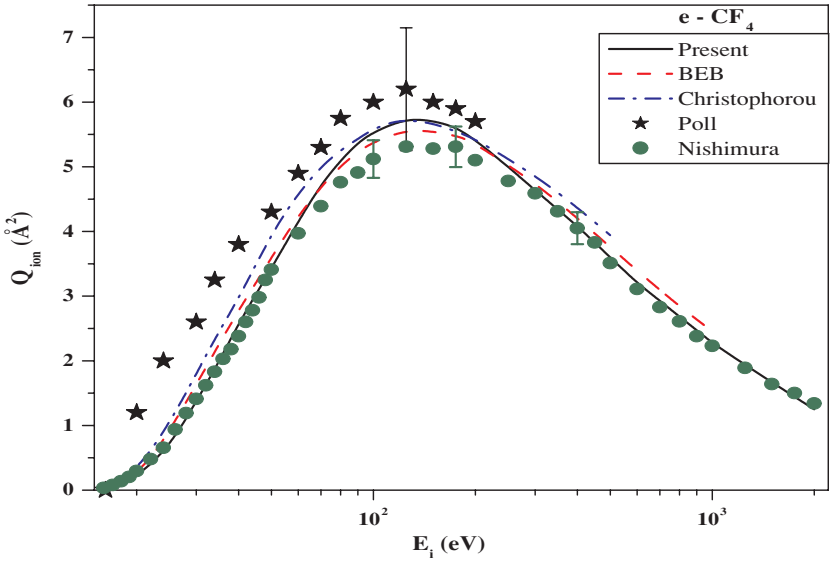

Figure 2. Total ionization cross sections for e–CF_4 scattering. The solid line represents the present results. Dash—BEB [33] (theory); dashed–dotted—Christophorou and Olthoff [41] (recommended); ⋆—Poll *et al* [42] (experiment); filled circles—Nishimura *et al* [43] (experiment).

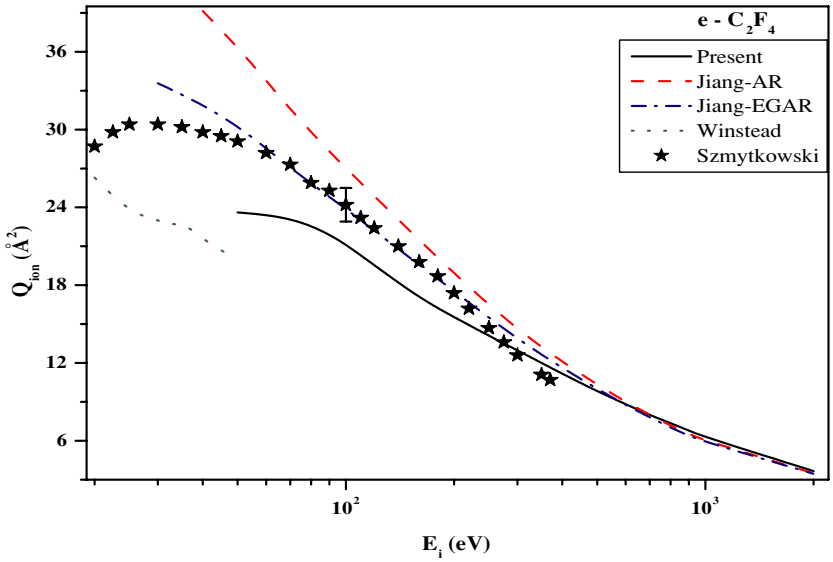

Figure 3. Total cross sections for e–C_2F_4 scattering. The solid line represents the present results. Dash—Jiang *et al* [32] (AR); dashed–dotted—Jiang *et al* [32] (EGAR); ⋆—Szmytkowski *et al* [44] (experiment); dotted—Winstead and McKoy [45] (SMC).

than the present estimates above 200 eV. Between 60 and 200 eV, these results [44] are in good agreement with the EGAR values of Jiang *et al* [32]. We have also plotted the calculated Q_T values from the Schwinger multi-channel (SMC) variational method of Winstead and McKoy [45] at low energies. These values are about 30% lower than the experiments of Szmytkowski *et al* [44].

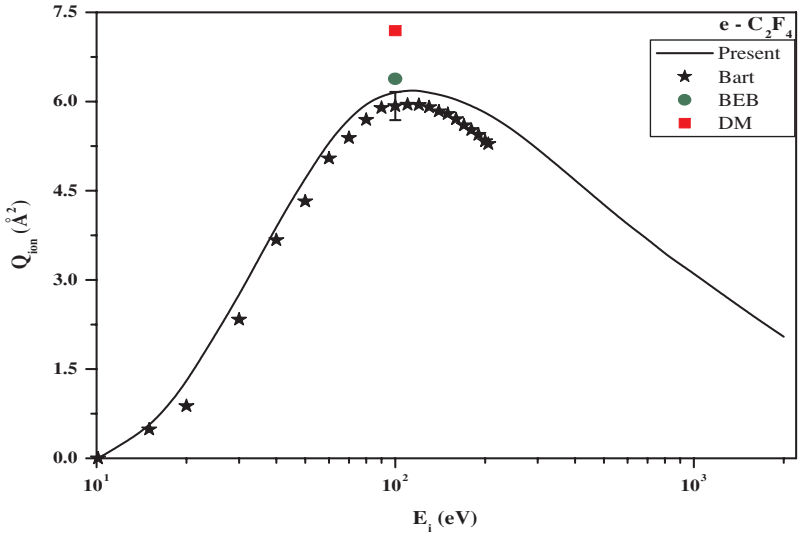

Figure 4. Total ionization cross sections for e–C_2F_4 scattering. The solid line represents the present results. ⋆—Bart *et al* [46] (experiment); filled circle—BEB [33] and filled square—DM from [46] (theory).

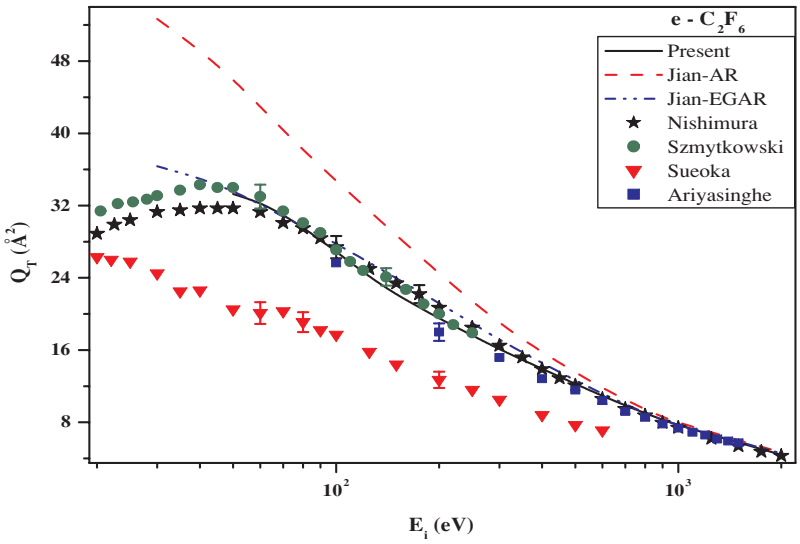

Figure 5. Total cross sections for e–C_2F_6 scattering. The solid line represents the present results. Dash—Jiang *et al* [32] (AR); dashed–dotted—Jiang *et al* [32] (EGAR); ⋆—Nishimura *et al* [39] (experiment); filled circles—Szmytkowski *et al* [47] (experiment); filled inverted triangles—Sueoka *et al* [48] (experiment) and filled squares—Ariyasinghe [49] (experiment).

Figure 4 shows the total ionization cross section of C_2F_4 together with the only available experimental values of Bart *et al* [46]. Two single points (the maximum values of $Q_{\rm ion}$(max)) calculated using the BEB [33] and DM methods [46] are also plotted. The peak values are higher than ours as well as the experimental values.

Total cross section values for C_2F_6 are plotted in figure 5 and compared with the experimental results of Nishimura *et al* [39], Szmytkowski *et al* [47], Sueoka *et al* [48]

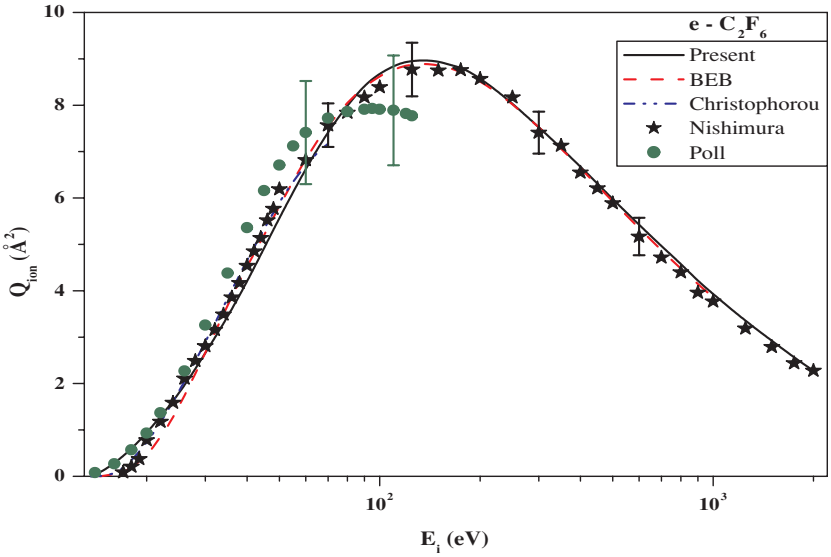

Figure 6. Total ionization cross sections for e–C_2F_6 scattering. The solid line represents the present results. Dash—BEB [33] (theory); dashed–dotted—Christophorou and Olthoff [50] (recommended); ⋆—Nishimura *et al* [43] (experiment); filled circles—Poll and Meichsner [42] (experiment).

and Ariyasinghe [49]. Our results are in agreement with all these experiments [39, 47, 49] at all energies. However, once again the values of Sueoka *et al* [48] are much lower and the discrepancy increases as the energy decreases. The additivity (AR) and modified additivity (EGAR—energy-dependent geometric additivity rule) results of Jiang *et al* [32] are also plotted. As was observed with the polyatomic C_2F_4 molecule, the AR values are much higher than the EGAR values, which are closer to the present results.

In figure 6, we present the total ionization cross sections of C_2F_6 along with BEB theory [33], recommended values from Christophorou and Olthoff [50], and the experimental data of Nishimura *et al* [43] and Poll and Meichsner [51]. Both theories and recommended values [50] lie within the experimental uncertainties. The agreement between the present theory, BEB method and experiments of Nishimura *et al* [43] is very good over the whole energy range. However the measurement of Poll and Meichsner [51] seems to underestimate the cross section above 80 eV.

In figure 7, the total cross sections, Q_T, for C_3F_8 are plotted. The present results indicate good agreement with the experiments of Nishimura *et al* [39] and Tanaka *et al* [52] at all energies, while the theoretical values of Jiang *et al* [32] are higher than these results. Once again as in the case of C_2F_4 and C_2F_6, EGAR is slightly higher than present results while AR of Jiang *et al* [32] significantly overestimates the cross section of all energies.

Estimated Q_{ion} for C_3F_8 are presented in figure 8 together with the experiments of Nishimura *et al* [43], Jiao *et al* [53] and Poll and Meichsner [51]. The BEB theory [33] and recommended values of Christophorou and Olthoff [54] are also compared with present results. The experiments of Nishimura [43] are in good agreement with present results and also with the BEB theory, except at the peak albeit still within their stated experimental error. The recommended values of Christophorou, the experimental values of Jiao *et al* and Poll *et al* closely follow our results from threshold to 70–80 eV but thereafter their results suggest a more strongly decreasing cross section. Jiao *et al* [53] also predict some structure between

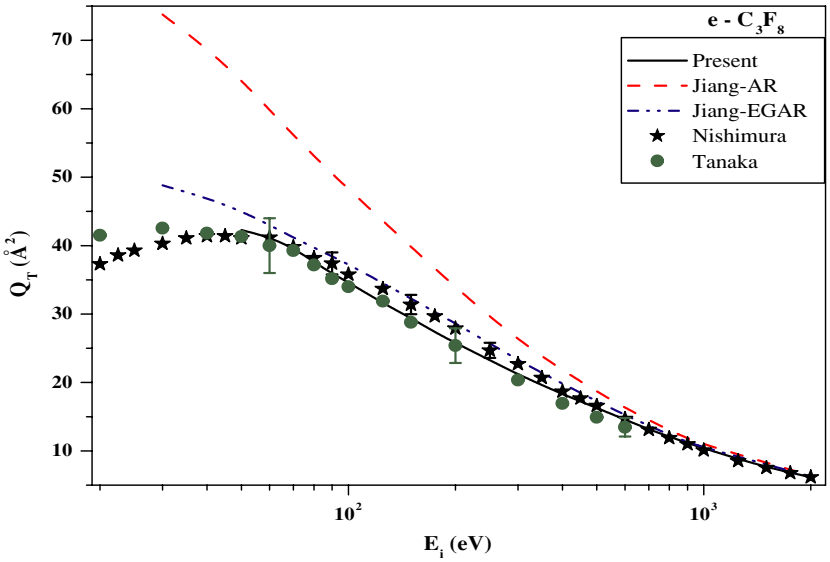

Figure 7. Total cross sections for e–C_3F_8 scattering. The solid line represents the present results. Dash—Jiang *et al* [32] (AR); dashed–dotted—Jiang *et al* [32] (EGAR);⋆—Nishimura *et al* [39] (experiment); filled circles—Tanaka *et al* [52] (experiment).

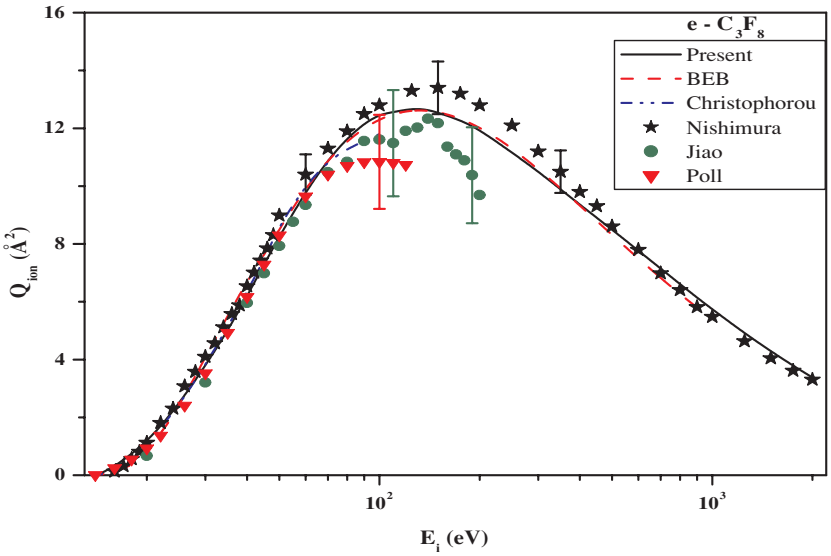

Figure 8. Total ionization cross sections for e–C_3F_8 scattering. The solid line represents the present results. Dash—BEB [33] (theory); dashed–dotted—Christophorou and Olthoff [54] (recommended); ⋆—Nishimura *et al* [43] (experiment); filled circles—Jiao *et al* [53] (experiment); filled inverted triangles—Poll and Meichsner [51] (experiment).

80 and 200 eV which we do not observe nor has such a feature been seen in any other Q_{ion} at these energies. However, as both experiments quote large error bars our results tend to fall within their quoted values over the entire energy range.

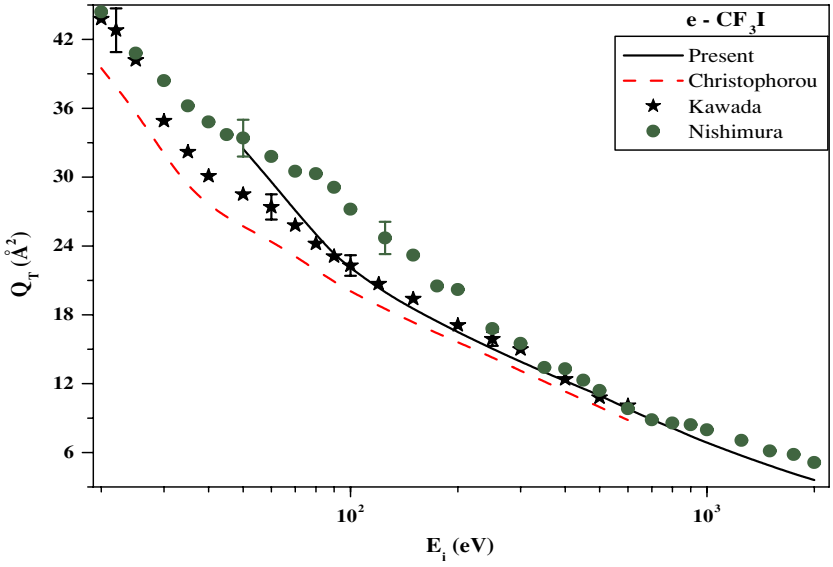

Figure 9. Total cross sections for e–CF_3I scattering. The solid line represents the present results. Dash—Christophorou and Olthoff [55] (recommended); ⋆—Kawada *et al* [56] (experiment); filled circles—Nishimura [57] (experiment).

In figure 9, we have plotted Q_T for CF_3I where, as already mentioned earlier, we have considered two centres, one at the centre of mass of the CF_3 branch and the other at the iodine atom. The recommended values of Christophorou and Olthoff [55] and the measurements of Kawada *et al* [56] and Nishimura [57] are also presented. Above 70 eV our results agree with the experiments of Kawada *et al* [56]. The values recommended by Christophorou [55] are in contrast lower than our results (although the shape of the cross section is similar). The experiments of Nishimura [57] are in good agreement with our values above 200 eV but below this energy show a structure at about 90 eV suggesting a different shape to the cross section.

In figure 10, we present Q_{ion} for CF_3I. These results are compared with DM theory [58] and experiments of Jiao *et al* [59]. The present results agree well with the experimental data, while the DM derived cross section peaks at lower energies and falls more rapidly at higher energies. This faster fall is a general feature of DM theory and has been pointed out in our earlier work [17].

The bar chart presented in figure 11, corresponding to the C_3F_8 molecule as an example, exhibits the relative contributions of various TCS to the Q_T of electron collisions at 150 eV. At this energy when the Q_{inel} is almost maximum, the distribution between ionization and electronic excitations can also be seen from this chart. The information (see figure 11) derived from the present calculations gives an approximate but overall theoretical picture of the above-threshold processes of electron scattering in this target. This will be useful for plasma molecules in view of incomplete data and existing discrepancies in the sum checks of various TCSs obtained from independent theories or experiments.

3.2. CF_x radicals

The cross sections for the CF_x ($x = 1$–3) radicals and their parent molecule CF_4 are compiled in table 3. Figures 12(a)–(c) correspond to the total ionization cross section (already published

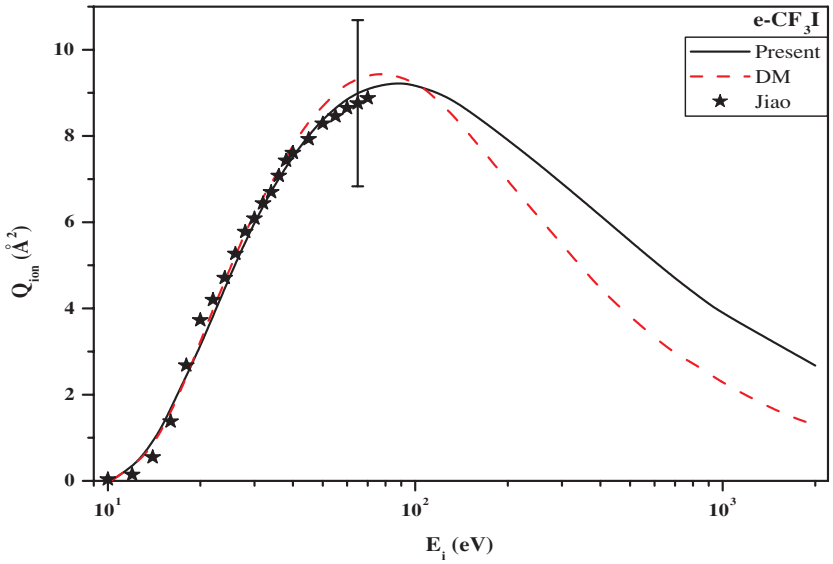

Figure 10. Total ionization cross sections for e–CF_3I scattering. The solid line represents the present results. Dash—DM [58] (theory); ⋆—Jiao *et al* [59] (experiment).

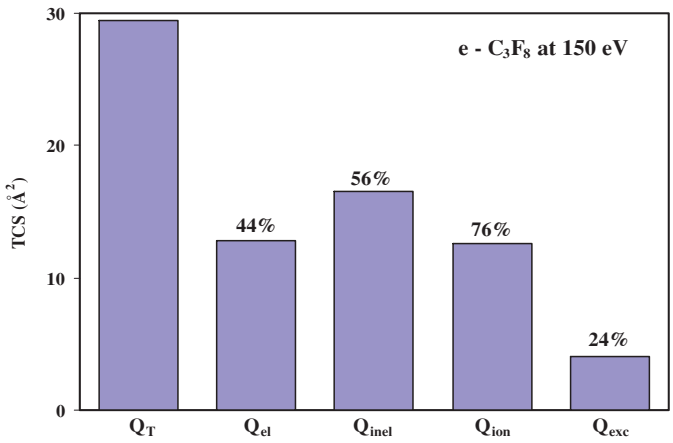

Figure 11. Relative contributions of various TCSs in e–C_3F_8 collisions at 150 eV.

in [17]) for the fluorocarbon radicals CF, CF_2 and CF_3, respectively. All the previous theoretical results [33, 60], as well as the present one [17], on these radicals are found to be on the higher side of the experimental data of Huo *et al* [61] except the siBED calculations by the same authors [61]. Nevertheless, it should be noted that their experimental data [61] involve a higher uncertainty of 25%. Calculations for $Q_{\rm inel}$ by Lee *et al* [62] (not shown here) are also on the higher side are as ours. The present and BEB values exceed the measurement and calculation of Huo *et al* [61] by more than 50%, while DM calculations [60] are less high. Notably, the experimental $Q_{\rm ion}$ of a CF_3 radical [61] and $Q_{\rm ion}$ of an individual carbon atom [63] are seen to be nearly equal, at the peak region, and this feature remains unexplained.

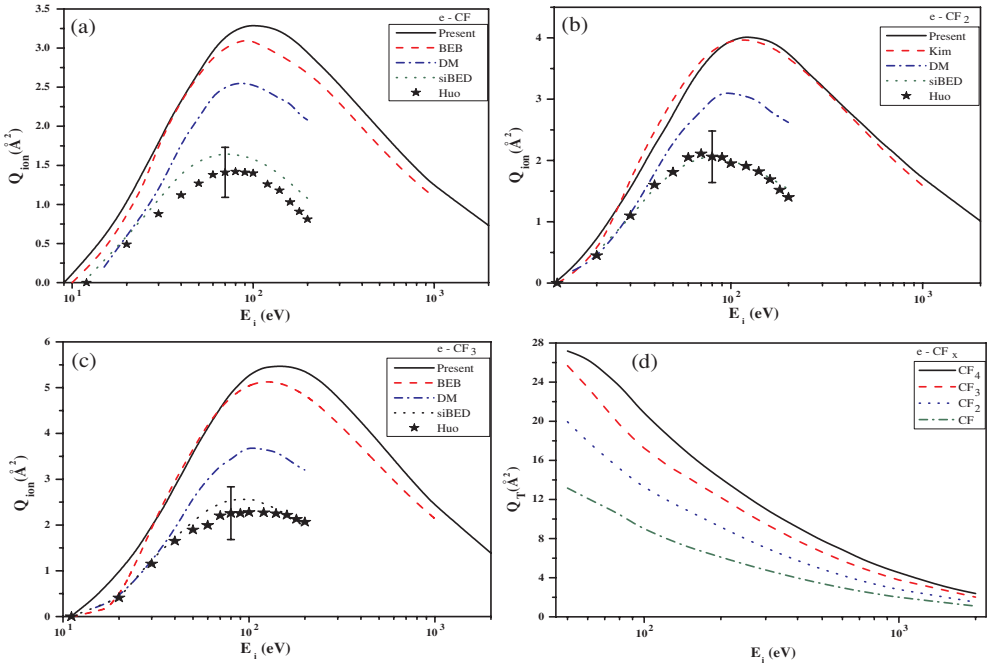

Figure 12. Electron impact ionization cross sections ($Q_{\rm ion}$) of (a) CF, (b) CF_2 and (c) CF_3 radicals. The solid line represent CSP-*ic* results; dashed—BEB [33]; dashed–dotted—DM [60]; dotted—siBED [61] and ⋆—experiment of Huo *et al* [61]. (d) The total cross sections ($Q_{\rm T}$) for CF_x radicals (dashed–dotted—CF, dotted—CF_2 and dashed—CF_3) and their parent molecule (solid curve) CF_4.

Figure 12(d) represents our $Q_{\rm T}$ on CF_x radicals along with the values from figure 1 for CF_4. No previous data are available for any of these radicals. The $Q_{\rm T}$ is found to be increasing nonlinearly with the increase in the number of fluorine atoms in the CF_x radical.

4. Conclusions

The present SCOP and CSP-ic methods to estimate total and ionization cross sections, respectively, have been used here for several plasma molecules. In this paper, our focus is on phenomena above the ionization threshold, typically from the energy at which $Q_{\rm ion}$ becomes appreciable. Even though the magnitude and position of $Q_{\rm ion}$ peak depends on the ionization potential, we find that it grows in accordance with the size of the molecule and number of electrons. This may be attributed to the comparable ionization potential (see table 1) for these stable species except for CF_4. We have also noted that the lower the ionization threshold the lower is the energy of the peak of $Q_{\rm ion}$ and the higher the peak magnitude. The general trend as above provides a useful guideline in understanding the electron impact ionization in a certain species of molecules, e.g., fluorocarbons. The present modified single centre approximation may not be accurate, but will be quite useful in 'guestimating' cross sections for heavier biomolecules.

The polarization and exchange models used in this paper are for intermediate and high energy scattering. This is the reason why we calculate the $Q_{\rm el}$ (and thus the $Q_{\rm T}$) above 50 eV only. In fact there is no single theory or model which will be equally successful at low as well

as high energies. However, in the case of inelastic cross section, the short-range interactions of the incident electron near the target charge cloud are important. We have found and mentioned earlier [16–19] that the Q_{inel} is hardly influenced (<1%) by the inclusion of the polarization potential.

The results obtained for e–CF_4 Q_{ion} and Q_{T} are in excellent agreement with previous theories and some of the experiments where available. For the molecules C_2F_6 and C_3F_8 there are only a few theories or experiments available. The present results seem to be in very good agreement with most of them, especially with the suggested values of Christophorou [11, 37, 41, 50, 54, 55]. In the case of C_2F_4 and CF_3I few data are available but from the results we obtained from the other molecules, we assume our values to be reliable.

Since the ionization threshold is lower for the transient radicals, the peak of Q_{ion} is higher in magnitude and occurs at relatively lower energies as compared to the parent stable molecules. Practically all the theories, including our own, are seen to overestimate the experimental Q_{ion} values, except the siBED model of the same group [61]. The discrepancy between the present results and the measured data is very high (>50%). Surprisingly, at the peak positions, the measured data for these radicals are just close to or even less than atomic carbon cross sections [17]. The Q_{T} presented in figure 12(d) for the CF_x radicals are the first calculations on these reactive species. Previous measurements are also not available for these radicals.

We hope that present calculations will help to initiate further theoretical calculations and, where practical, experimental effort, on characterizing electron collision processes with plasma molecules.

Acknowledgments

BKA thanks the ACU, UK, for a Commonwealth Scholarship and CSIR, India, for a Senior Research Fellowship award. We also thank Dr Elaine Moore (at the Open University, UK) for calculating the electric dipole polarizabilities required in our calculation and Professor Hiroyuki Nishimura for providing us with his latest experimental values prior to publication.

References

[1] Matsuura T, Murota J, Sawada Y and Ohmi T 1993 *Appl. Phys. Lett.* **63** 2803
[2] Matsuura T, Sugiyama T and Murota J 1998 *Surf. Sci.* **402–404** 202
[3] Matsuura T, Honda Y and Murota J 1999 *Appl. Phys. Lett.* **74** 3573
[4] Mason N J and Itoh H (ed) 2003 *Report of EU-JAPAN Joint Symposium on Plasma Processing* (organized by Open University, UK and Association of Super-Advanced Electronics Technologies–Japan)
[5] Hatano Y 2000 *Adv. At. Mol. Opt. Phys.* **43** 231
[6] Makabe T 2002 *Advances in Low Temperature RF Plasmas—Bases for Process Design* (Amsterdam: Elsevier)
[7] 1991 *Plasma Processing of Materials: Scientific Opportunities and Technological Challenges* (Washington, DC: National Research Council, National Academy Press)
1996 *Database Needs for Modelling and Simulation of Plasma Processing* (Washington, DC: National Research Council, National Academy Press)
[8] De Bleecker K, Herrebout D, Bogaerts A, Gijbels R and Descamps P 2003 *J. Phys. D: Appl. Phys.* **36** 1826
[9] Samukawa S and Mukai 1999 *J. Vac. Sci. Technol.* A **17** 5
[10] Tanaka H and Inokiti M 2000 *Adv. At. Mol. Opt. Phys.* **43** 1
[11] Christophorou L G and Qithoff J K 2003 *Fundamental Electron Interactions with Plasma Processing Gases* (New York: Kluwer/Plenum)
[12] Whelan C T and Mason N J (ed) 2003 *Electron Scattering from Atoms, Molecules, Nuclei and Bulk Matter* (New York: Plenum)
[13] Burke P G and Berrington K A 1993 *Atomic and Molecular Processes—An R-Matrix Approach* (Bristol: Institute of Physics Publishing)

[14] Morgan L A, Tennyson J and Gillan C J 1998 *Comput. Phys. Commun.* **114** 120
[15] Joshipura K N and Antony B K 2001 *Phys. Lett.* A **289** 323
[16] Joshipura K N, Antony B K and Vinodkumar M 2002 *J. Phys. B: At. Mol. Opt. Phys.* **35** 4211
[17] Joshipura K N, Vinodkumar M, Antony B K and Mason N J 2003 *Eur. Phys. J.* D **23** 81
[18] Joshipura K N, Minaxi V, Limbachiya C G and Antony B K 2004 *Phys. Rev.* A **69** 022705
[19] Antony B K, Joshipura K N and Mason N J 2004 *Int. J. Mass Spectrom.* **233** 207
[20] Karna S P and Dupuis M 1991 *J. Comput. Chem.* **12** 487
[21] Schmidt M W *et al* 1993 *J. Comput. Chem.* **14** 1347
[22] Sadlej A J 1988 *Collec. Czech. Chem. Commun.* **53** 1995
[23] Sadlej A J 1992 *Theor. Chim. Acta* **81** 339
[24] Helgaker T *et al* 2001 *Dalton, A Molecular Electronic Structure Program,* Release 1.2
[25] Barysz M *et al* 2002 *MOLCAS* Version 5.4, ed K Andersson Lund University, Sweden
[26] Zecca A, Karwasz G P, Brusa R S and Szmytkowski C 1992 *Phys. Rev.* A **45** 2777
[27] Joshipura K N and Vinodkumar M 1997 *Z. Phys.* D **41** 133
[28] Lide R 2003 *CRC Handbook of Chemistry and Physics* (Boca Raton, FL: CRC Press)
[29] http://Webbook.Nist.gov
[30] Staszewska D, Schwenke D W, Thirumalai D and Truhlar D G 1984 *Phys. Rev.* A **29** 3078
[31] Joachain C J 1983 *Quantum Collision Theory* (Amsterdam: North-Holland)
[32] Jiang Y, Sun J and Wan L 2000 *Phys. Rev.* A **62** 062712
[33] Kim Y-K, Hwang W, Weinberger N M, Ali M A and Rudd M E 1997 *J. Chem. Phys.* **106** 1026
[34] Kim Y-K and Rudd M E 1994 *Phys. Rev.* A **50** 3954
NIST Web site http://physics.nist.gov/PhysRefData/Ionization
[35] Probst M, Deutsch H, Becker K and Märk T D 2001 *Int. J. Mass Spectrom.* **206** 13, and references therein
[36] Jiang Y, Jinfeng S and Lide W 1995 *Phys. Rev.* A **52** 398
[37] Christophorou L G, Qithoff J K and Rao M V V S 1996 *J. Phys. Chem. Ref. Data* **25** 1341
[38] Zecca A, Karwasz G P and Brusa R S 1992 *Phys. Rev.* A **46** 3877
[39] Nishimura H, Nishimura F, Nakamura Y and Okuda K 2003 *J. Phys. Soc. Japan* **72** 1080
[40] Sueoka O, Mori S and Hamada A 1994 *J. Phys. B: At. Mol. Opt. Phys.* **27** 1453
[41] Christophorou L G and Olthoff J K 1999 *J. Phys. Chem. Ref. Data* **28** 967
[42] Poll H U, Winkler C, Margreiter D, Grill V and Märk T D 1992 *Int. J. Mass Spectrom. Ion Process.* **112** 1
[43] Nishimura H, Huo W M, Ali M A and Kim Y K 1999 *J. Chem. Phys.* **110** 3811
[44] Szmytkowski C, Kwitnewski S and Ptasiska-Denga E 2003 *Phys. Rev.* A **68** 032715
[45] Winstead C and McKoy V 2002 *J. Chem. Phys.* **116** 1380
[46] Bart M, Harland P W, Hudson J E and Vallance C 2001 *Phys. Chem. Chem. Phys.* **3** 800
[47] Szmytkowski C, Mozejko P, Kasperski G and Ptasiska-Denga E 2000 *J. Phys. B: At. Mol. Opt. Phys.* **33** 15
[48] Sueoka O, Makochekanwa C and Kawate H 2002 *Nucl. Instrum. Methods* B **192** 206
[49] Ariyasinghe W M 2003 *Radiat. Phys. Chem.* **68** 79
[50] Christophorou L G and Olthoff J K 1998 *J. Phys. Chem. Ref. Data* **27** 1
[51] Poll H U and Meichsner J 1987 *Contrib. Plasma Phys.* **27** 259
[52] Tanaka H, Tachibana Y, Kitajima M, Sueoka O, Takaki H, Hamada A and Kimura M 1999 *Phys. Rev.* A **59** 2006
[53] Jiao C Q, Garscadden A and Haaland P D 2000 *Chem. Phys. Lett.* **325** 203
[54] Christophorou L G and Olthoff J K 1998 *J. Phys. Chem. Ref. Data* **27** 889
[55] Christophorou L G and Olthoff J K 2000 *J. Phys. Chem. Ref. Data* **29** 553
[56] Kawada M K, Sueoka O and Kimura M 2000 *Chem. Phys. Lett.* **330** 34
[57] Nishimura H 2003 Private communication
[58] Onthong U, Deutsch H, Becker K, Matt S, Probst M and Märk T D 2002 *Int. J. Mass Spectrom.* **214** 53
[59] Jiao C Q, Ganguly B, DeJoseph D A Jr and Garscadden A 2001 *Int. J. Mass Spectrom.* **208** 127
[60] Deutsch H, Becker K, Matt S and Märk T D 2000 *Int. J. Mass Spectrom.* **197** 37
[61] Huo W M, Tarnovsky V and Becker K H 2002 *Chem. Phys. Lett.* **358** 328
[62] Lee M-T, Iga I, Brescansin L M, Machado L E and Machado F B C 2002 *Phys. Rev.* A **66** 012720
[63] Margreiter D, Deutsch H and Märk T D 1994 *Int. J. Mass Spectrom. Ion. Process.* **139** 127